The H1 Lead/Scintillating–Fibre Calorimeter

H1 SPACAL Group

Abstract

The backward region of the H1 detector has been upgraded in order to provide improved measurement of the scattered electron in deep inelastic scattering events. The centerpiece of the upgrade is a high–resolution lead/scintillating–fibre calorimeter.

The main design goals of the calorimeter are: good coverage of the region close to the beam pipe, high angular resolution and energy resolution of better than 2% for 30 GeV electrons. The calorimeter should be capable of providing coarse hadronic energy measurement and precise time information to suppress out–of–time background events at the first trigger level. It must be compact due to space restrictions.

These requirements were fulfilled by constructing two separate calorimeter sections. The inner electromagnetic section is made of 0.5 mm scintillating plastic fibres embedded in a lead matrix. Its lead–to–fibre ratio is 2.3:1 by volume. The outer hadronic section consists of 1.0 mm diameter fibres with a lead–to–fibre ratio of 3.4:1.

The mechanical construction of the new calorimeter and its assembly in the H1 detector are described.

H1 SPACAL Group

R.-D. Appuhn[4], C. Arndt[4], E. Barrelet[10], R. Barschke[4], U. Bassler[10], V. Boudry[9],
R. Buchholz[4], F. Brasse[4], D. Bruncko[6], S. Chechelnitski[8] B. Claxton[14], G. Cozzika[3],
J. Cvach[11], S. Dagoret-Campagne[10], W.D. Dau[15], H. Deckers[2], T. Deckers[2], F. Descamps[10],
M. Dirkmann[2], J. Dowdell[14], V. Efremenko[8], E. Eisenhandler[7], A.N. Eliseev[17], G. Falley[4],
J. Ferencei[6], B. Fominykh[8], K. Gadow[4], U. Goerlach[4,α], L.A. Gorbov[17], I. Gorelov[8],
M. Grewe[2], L. Hajduk[13], I. Herynek[11], J. Hladký[11], M. Hütte[2], H. Hutter[2], W. Janczur[13],
J. Janoth[5], L. Jönsson[16], H. Kolanoski[2], V. Korbel[4], F. Kriváň[6], D. Lacour[10], F. Lamarche[9],
M.P.J. Landon[7], B. Laforge[3], J.-F. Laporte[3], F. Lehner[4], R. Maraček[6], K. Meier[5], A. Meyer[4],
A. Migliori[9], F. Moreau[9], G. Müller[4], P. Murín[6], V. Nagovizin[8], T.C. Nicholls[1], D. Ozerov[8],
E. Perez[3], J.P. Pharabod[9], R. Pöschl[2], K. Rybicki[13], A. Rostovtsev[8], C. Royon[3], S. Schleif[5],
A. Schuhmacher[2], A. Semenov[8], V. Shekelyan[8], Y. Sirois[9], P.A. Smirnov[17,c], V. Solochenko[8],
J. Špalek[6], S. Spielmann[9], H. Steiner[4,β], J. Stiewe[5], M. Taševský[12], V. Tchernyshov[8],
K. Thiele[4], E. Tzamariudaki[4], S. Valkár[12], D. VanDenPlas[9], G. Villet[3], K. Wacker[2],
A. Walther[2], M. Weber[5], D. Wegener[2], T. Wenk[2], J. Žáček[12], A. Zhokin[8] and K. Zuber[5]

[1] *School of Physics and Space Research, University of Birmingham, Birmingham, UK[a]*
[2] *Institut für Physik, Universität Dortmund, Dortmund, Germany[b]*
[3] *CEA, DSM/DAPNIA, CE-Saclay, Gif-sur-Yvette, France*
[4] *DESY, Hamburg, Germany[b]*
[5] *Institut für Hochenergiephysik, Universität Heidelberg, Heidelberg, Germany[b]*
[6] *Institute of Experimental Physics, Slovak Academy of Sciences, Košice, Slovak Republic[c,d]*
[7] *Queen Mary and Westfield College, London, UK[a]*
[8] *Institute for Theoretical and Experimental Physics, Moscow, Russia[e]*
[9] *LPNHE, Ecole Polytechnique, IN2P3-CNRS, Palaiseau, France*
[10] *LPNHE, Universités Paris VI and VII, IN2P3-CNRS, Paris, France*
[11] *Institute of Physics, Czech Academy of Sciences, Prague, Czech Republic[c,f]*
[12] *Nuclear Center, Charles University, Prague, Czech Republic[c,f]*
[13] *Insitute for Nuclear Physics, Cracow, Poland[g]*
[14] *Electronics Division, Rutherford Appleton Laboratory, Chilton, Didcot, UK[a]*
[15] *Institut für Reine und Angewandte Kernphysik, Universität Kiel, Kiel, Germany[b]*
[16] *Physics Department, University of Lund, Sweden[h]*
[17] *Lebedev Physical Institute, Moscow, Russia*

1 Introduction

The electron–proton collider HERA at DESY is a unique facility that has opened a new kinematic range in lepton–nucleon scattering. The measurement of the proton structure function at very small values of the Bjorken scaling variable x has become an area of key interest at HERA. This requires a precise measurement of the energy and the polar angle of electrons scattered into the backward region of the H1 detector — the angular region opposite to the direction of the incoming proton beam.

To fulfil this task optimally, the H1 collaboration undertook an extensive upgrade program by constructing and installing three new detectors: a silicon tracker, a planar drift chamber and a lead/scintillating–fibre calorimeter [1]. The existing detectors [2] in the backward region of the H1 detector were replaced.

This paper describes the design, construction and assembly of the new calorimeter, which was installed into the H1 detector in the winter shutdown 1994/95. More specific information on the hadronic section may be obtained from [3]. A detailed review of the electronics and of the calorimeter performance in test beam measurements can be found in [4]–[7].

2 Physics Requirements

The construction of the new backward calorimeter aims for enlarged angular acceptance and better control of systematic errors in the determination of the proton structure function at low values of x. The detailed physics requirements are motivated below and are summarized in Table 1.

The acceptances of the new and the old calorimeter are compared in Figure 1. The new calorimeter extends to x values of the order of 10^{-5} by detecting electrons with scattering angles as large as 177.5° with respect to the incident proton direction. Even lower values of x are accessible by shifting the interaction points of the electron–proton collisions.

An important contribution to the systematic error of structure function measurements comes from the determination of the kinematical variables x, y and Q^2, which can be reconstructed from the electron energy and scattering angle [8]. At small values of y, the x resolution is strongly affected by energy resolution. Similarly at large scattering angles the Q^2 resolution is very sensitive to the angular resolution. The energy resolution of the electromagnetic calorimeter should therefore be better than 2% for electron energies of 30 GeV, and the angular resolution should be 1–2 mrad which corresponds to a position resolution of a few millimeters [1]. Besides entering the kinematic variable reconstruction, a particle's impact position at the calorimeter may also be compared to track extrapolations. Since the kinematic variables can also be calculated using hadronic particles only, the detector should also provide a hadronic energy measurement for redundancy.

An important experimental challenge is the reliable separation of electrons and charged hadrons at low energies. This is required to suppress fake electrons from photoproduction events where the scattered electron escapes in the beam pipe. Photoproduction events are several orders of magnitude more abundant than deep inelastic scattering events. The design goal of the calorimeter is a $\pi^{\pm}$ rejection factor $\epsilon_e/(1 - \epsilon_\pi)$ larger than 100, where ϵ_e and ϵ_π are the electron and the charged pion identification efficiency, respectively.

At HERA the rate of beam–gas and beam–wall background events caused by the proton beam is large. Efficient reduction of these events at the first trigger level is essential. We want to veto upstream beam–related background events by exploiting their time–of–flight difference
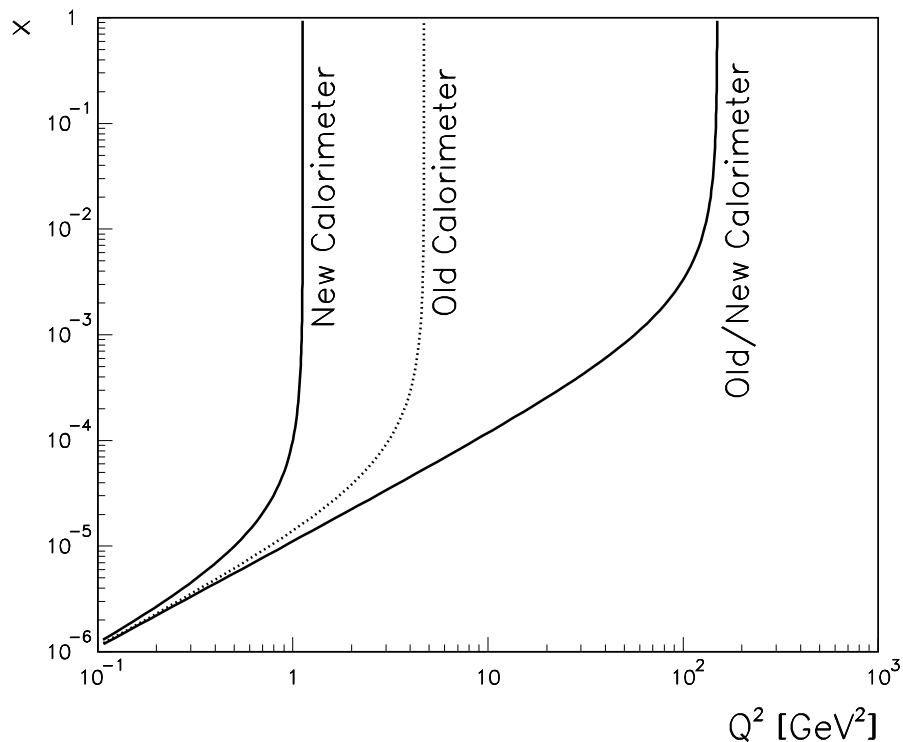
Figure 1: The acceptance of the new and the old calorimeter in the x–Q^2 plane. The acceptance region of the new calorimeter is given by the two full lines. The minimum x–Q^2 values accessible with the old calorimeter are given by the dotted line.

of $\sim$ 10 ns compared to events originating from the nominal interaction point. Thus a time resolution of the order of 1 ns independent of the particle energy, i. e. for high–energy electrons, interacting pions and minimum ionizing particles, is required. In addition, a sophisticated electron trigger of high granularity is needed to be able to cope with the expected increase of the HERA luminosity. The trigger concept is described in more detail in [4].

Important practical constraints were imposed by the limited space that was available for the new calorimeter, which must fit into the existing H1 detector. In addition, the detector has to operate within a strong magnetic field of 1.0 Tesla.

Table 1: Design requirements of the calorimeter

Acceptance	$153° < \theta < 177.5°$
σ /E	$7\%/\sqrt{E} \oplus 1\%$
e/π separation	$\epsilon_e/(1 - \epsilon_\pi) > 100$
Time resolution	< 1 ns
Position resolution	a few mm

4

3   Calorimeter Design

The main detector alternatives considered to fulfil the requirements listed in section 2 were a lead/scintillating–fibre calorimeter (SPACAL) and a lead fluoride crystal calorimeter. An R&D program for both options was started. Prototype studies with four $21 \times 21 \times 170$ mm^3 lead fluoride crystals showed encouraging results in electromagnetic resolution [9]. We opted for a lead/scintillating–fibre calorimeter, however, due to the anticipated high cost of the crystals and their inferior hadronic energy resolution.

The concept of lead/scintillating–fibre calorimeters came up with the advent of suitable optical fibres. Since then considerable experience with this new technique has been gained [10]–[14]. A large scale scintillating–fibre calorimeter with excellent electromagnetic energy resolution was built by the JETSET experiment at LEAR [15], and an electromagnetic scintillating–fibre calorimeter for operation at DAΦNE is currently being constructed by the KLOE collaboration [16]. Besides these experiments with moderate particle energies compared to electron–proton collisions at HERA, intensive research programs were started at CERN to investigate the use of scintillating–fibre calorimeters at LHC [17, 18]. These efforts resulted in various prototypes, with different choices of fibre diameters and lead–to–fibre volume ratios adapted to the specific design goals.
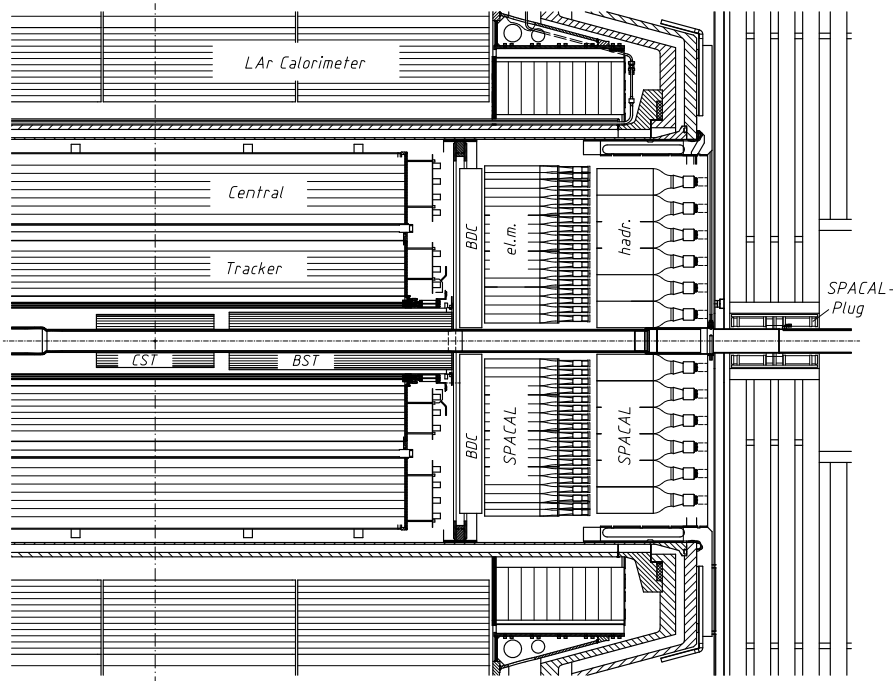
Figure 2: Partial side view of the H1 detector showing the position of the new calorimeters (SPACAL). The figure also shows the new Backward Silicon Tracker (BST) and the Backward Drift Chamber (BDC). The electron beam direction is from left to right.

Our detector layout is illustrated in Figure 2, showing a side view of the backward part of the H1 detector. The calorimeter consists of two separate sections, an inner electromagnetic and an outer hadronic section. The hadronic section is completed by the backward plug calorimeter which is located in the iron return yoke of the H1 magnet.

The separation into two calorimeters allows optimization of the electromagnetic energy resolution while maintaining coverage of hadronic particles and longitudinal segmentation. The comparison of the energy depositions in the two sections enhances the electron–pion separation capability. In addition, independent trigger information is provided by the hadronic calorimeter.

The fibre diameter of the electromagnetic section is 0.5 mm, with a lead–to–fibre ratio of 2.3:1 by volume. Due to the small fibre diameter a high sampling frequency is obtained, which allows us to obtain the design energy resolution with a sampling term close to $7\%/\sqrt{E(\mathrm{GeV})}$ [6]. The choice of the lead–to–fibre ratio is a compromise between aiming for an even smaller sampling term or for a more compact calorimeter. Our choice of these parameters is a novel approach which has not been adopted before.

The active volume of the electromagnetic calorimeter is 250 mm deep, corresponding to 28 radiation lengths. Test beam measurements have shown that longitudinal energy leakage is negligible for 30 GeV electron showers [6]. The cell cross section is 40.5×40.5 mm^2. The high granularity is well matched to the Molière radius of 25.5 mm to ensure good electron–pion separation and good position resolution.

The scintillation light is read out by photomultipliers to achieve 1 ns time resolution and a low noise level. We chose mesh–type photomultipliers capable of operating within the strong magnetic field. More details on the photomultipliers are given in section 4.

For the hadronic section, the fibre diameter is 1 mm and the lead–to–fibre ratio is 3.4:1. The hadronic calorimeter section adds 1.02 interaction lengths of material to the electromagnetic section, which is 1.0 interaction lengths deep. Its weight was required not to exceed 4 tons to keep the load put on the H1 liquid argon cryostat reasonably small. In addition, the depth of the hadronic calorimeter is constrained by the iron return yoke of the H1 magnet. A cell cross section of 119.3×119.0 mm^2 was chosen, corresponding to the lateral dimensions of hadronic showers. Again, mesh–type photomultipliers are used.

A summary of the main construction parameters is given in Table 2.

Table 2: Construction parameters of the calorimeter.

	Electromagnetic section	Hadronic section
Fibre diameter	0.5 mm	1.0 mm
Lead/fibre ratio	$2.3 : 1$	$3.4 : 1$
Number of channels	1192	136
Size of standard cell	40.5×40.5 mm^2	119.3×119.0 mm^2
Active length	250 mm	250 mm
Radiation length	9.0 mm	8.5 mm
Interaction length	250 mm	246 mm
Molière radius	25.5 mm	24.5 mm
Lead–fibre density	7.3 g/cm^3	7.7 g/cm^3

4   Electromagnetic Section

The cell structure of the electromagnetic calorimeter is illustrated in Figure 3. The calorimeter is centered around the beam pipe. The smallest construction units of the detector are 2–cell

modules. Sets of eight 2–cell modules are combined to form square 16–cell modules which represent the main building blocks of the detector.

The innermost module, which contains the opening for the beam pipe, is called the insert module. It is used to measure electrons at small scattering angles with respect to the incoming electron beam and to detect shower leakage into the beam pipe. Another set of specially tailored modules is positioned at the outer border of the detector to approximate the circular shape of the 800 mm diameter aluminium frame which encloses the calorimeter modules. The four 16–cell modules on top of the insert module must not put pressure onto the HERA beam pipe. These modules are therefore held by a loop of four 2×25 μm thick steel bands fixed at the top of the aluminium frame.

The construction of the 2–cell modules, of the 16–cell modules, of the insert module, and the detector assembly is described in detail in the following subsections.
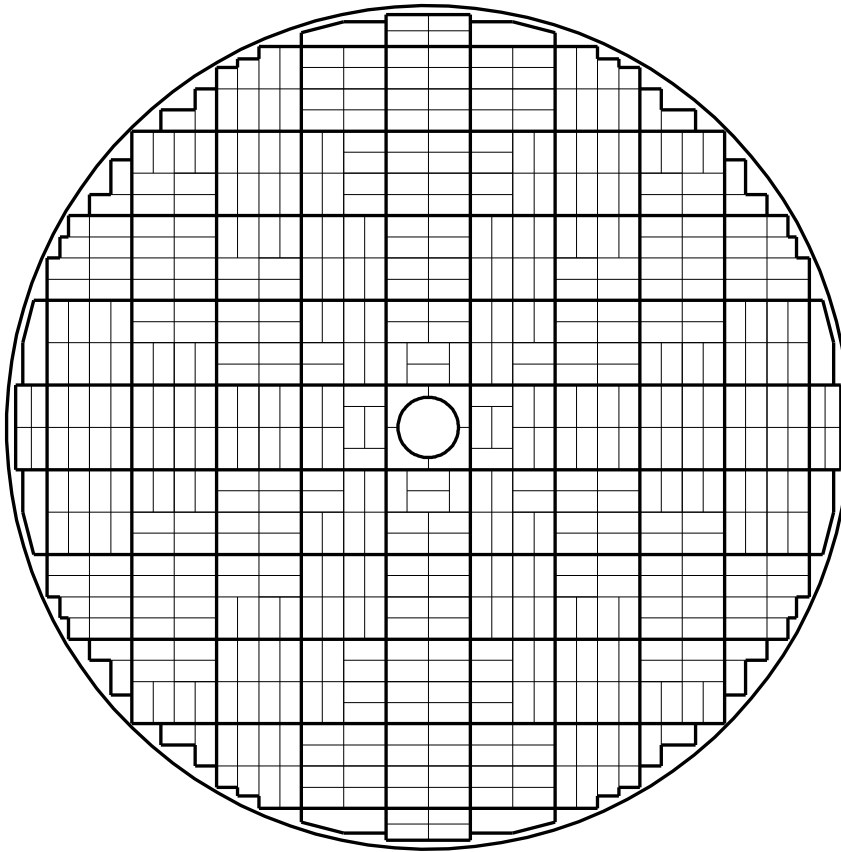
Figure 3: r–ϕ view of the electromagnetic calorimeter. The borders of the 16–cell modules are given by bold lines. The arrangement of the 2–cell modules, which is motivated in section 4.3, is indicated by thin lines.

4.1   Lead Plate Production

The small lead–to–fibre ratio of 2.3:1 and the groove dimensions and tolerances which are given by the fibre diameter of 0.5 mm made the production of the lead plates a difficult task. The

lead profile chosen for the electromagnetic section is shown in Figure 4. Each plate contains 90 grooves of 0.52 mm diameter. The height of the lead plates is 0.78 mm. The minimal lead thickness below a fibre groove is 0.24 mm. The grooves were made only in the top of the plate, which simplified the insertion of the fibres.
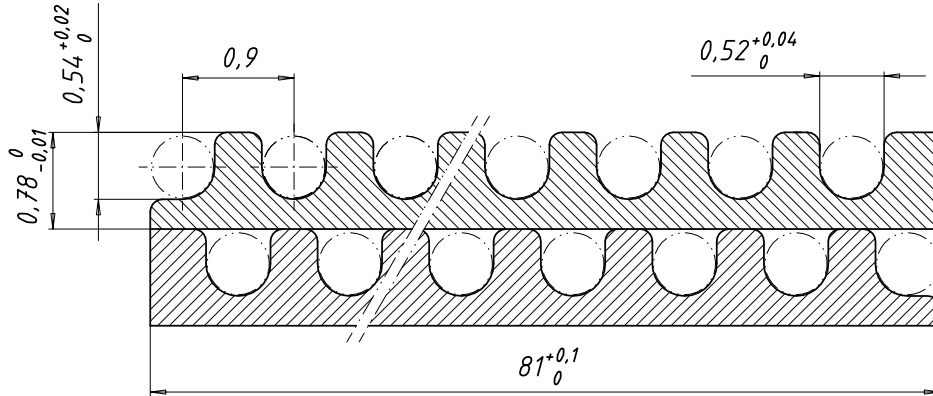

Figure 4: Cross section of two lead plates.

The main plate production techniques that have been utilized in lead/scintillating–fibre calorimetry are extrusion, machining and rolling [15]–[18]. Extrusion was excluded in our case because the lead plates were too thin, while machining is expensive and slow. Therefore we chose rolling and constructed a rolling machine. The raw material is soft lead without any added antimony. A drawing of the rolling machine is displayed in Figure 5. The first pair of rollers defines the thickness of the lead plates, and the second pair of rollers makes the groove profile. After passing the rollers the lead plates are cut and are cleaned in an ultra–sonic bath.

The mechanical precision of the lead profile is essential for the quality of the detector. The nominal lead sheet height of 0.78 mm is reproduced with a precision of better than 10 μm. This precision is required to keep within the mechanical tolerances of the 16–cell modules, which consist of 208 stacked plates, close to 0.1 mm and to avoid resulting inhomogenities at the module borders.

4.2 Scintillating Fibres

The quality of the scintillating fibres has considerable impact on the detector properties. We therefore started an extensive test program investigating fibres from various companies. Finally, we chose BICRON BCF–12 [19] fibre, which emits blue light with an emission peak near 430 nm. The fibre consists of a polystyrene–based core doped with scintillator and of a 20 μm thick acrylic cladding. The refractive indices of the core and the cladding are 1.6 and 1.49, respectively. Light transport occurs by total reflection either on the core–cladding surface or on the cladding–air surface, depending on the emission angle of the scintillation light.

Among the fibre properties which we studied in our test program were the scintillation light yield, the fibre attenuation length and the radiation hardness of the fibres [20]. Most of these properties were measured by illuminating a sample of fibres with a ^{90}Sr β–source and recording the scintillation light with a photomultiplier placed at one fibre end. The cladding light, which

Height (mm)	0,7±0,05	0,6±0,02	0,78±0,01	0,78±0,01	0,78±0,01
Width (mm)	86±0,1	86±0,5	81±0,2	81±0,1	81±0,1
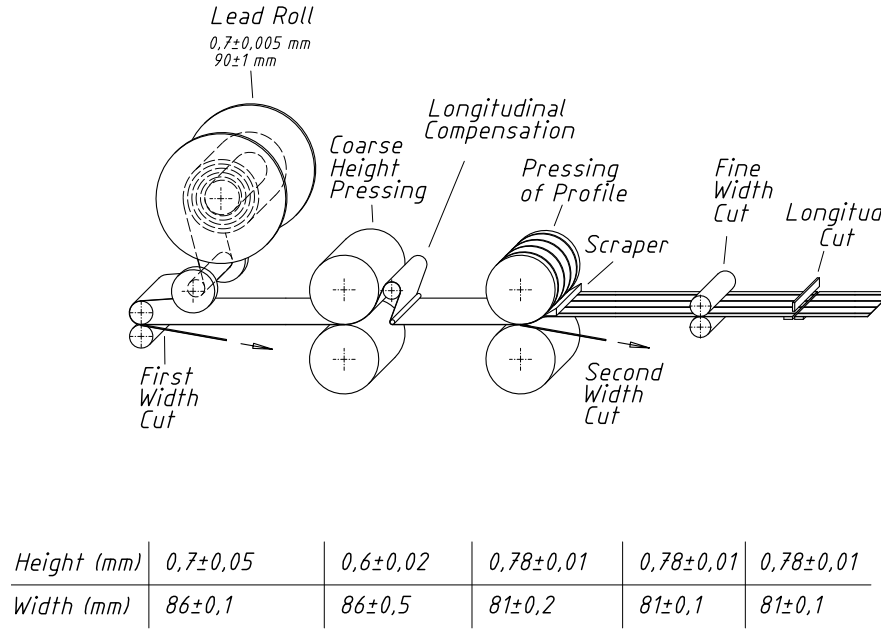
Figure 5: Drawing of the rolling machine. The table gives the height and the width of the lead after each pressing are cutting step.

has a very short attenuation length, was suppressed by blackening the outer surface of the fibre near the photomultiplier.
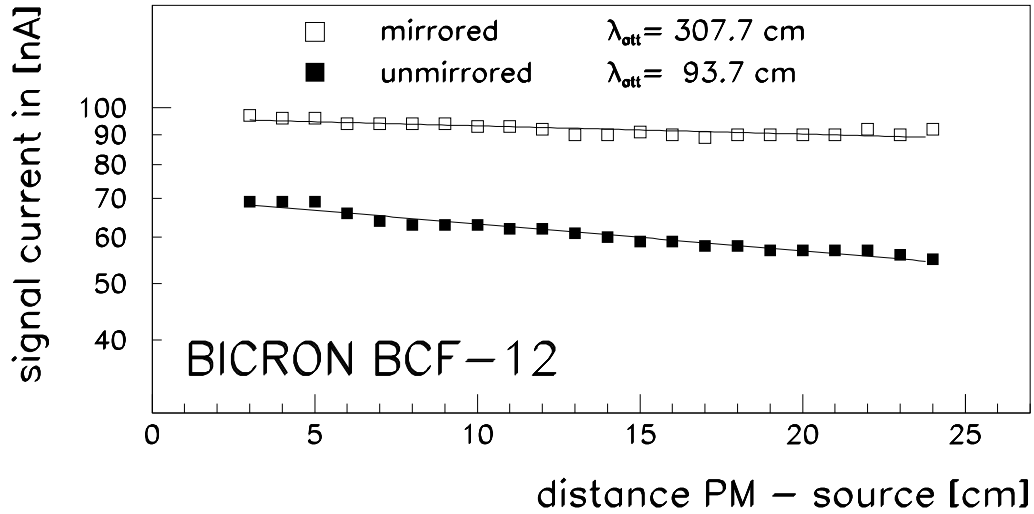
Figure 6: Determination of the light yield and attenuation length for mirrored and unmirrored BCF–12 fibres.

In Figure 6, the measured light yield is shown as a function of the β–source position for both mirrored and unmirrored fibre ends. The mirrors consist of a thin layer of vacuum–vapourized deposited aluminium. It is clear that both the light intensity and the attenuation length are

9

considerably increased by the mirroring. The attenuation length for 25 cm long mirrored BCF–12 fibres is found to be larger than 3 m. This ensures that fluctuations of the electromagnetic shower position as well as the logarithmic energy dependence of the shower–maximum position do not influence the detector response significantly. All calorimeter fibres were consequently mirrored. Before mirroring the fibre ends were machined with a diamond tool to ensure a flat optical surface. We did not polish the fibre in order to avoid possible long–term damage related to the polishing medium.

During construction, a sample of 30 fibres per delivered fibre batch was measured routinely [21]. Fibres belonging to one batch are drawn from the same source material and so have similar optical properties. Thus we took care not to mix fibres from different batches for a given cell. If mixing could not be avoided batches with similar properties were mixed.

We find that typical fibre–to–fibre fluctuations of the light yield within a batch of fibres are below 5%. Our detector simulations have shown that a fluctuation of 10% results in a constant term to the energy resolution of the order of 1%. Similarly an attenuation length of 1 m would contribute 1% to this constant term. Thus the fibre properties, in terms of both light yield fluctuations and attenuation length are fully acceptable for our purpose.
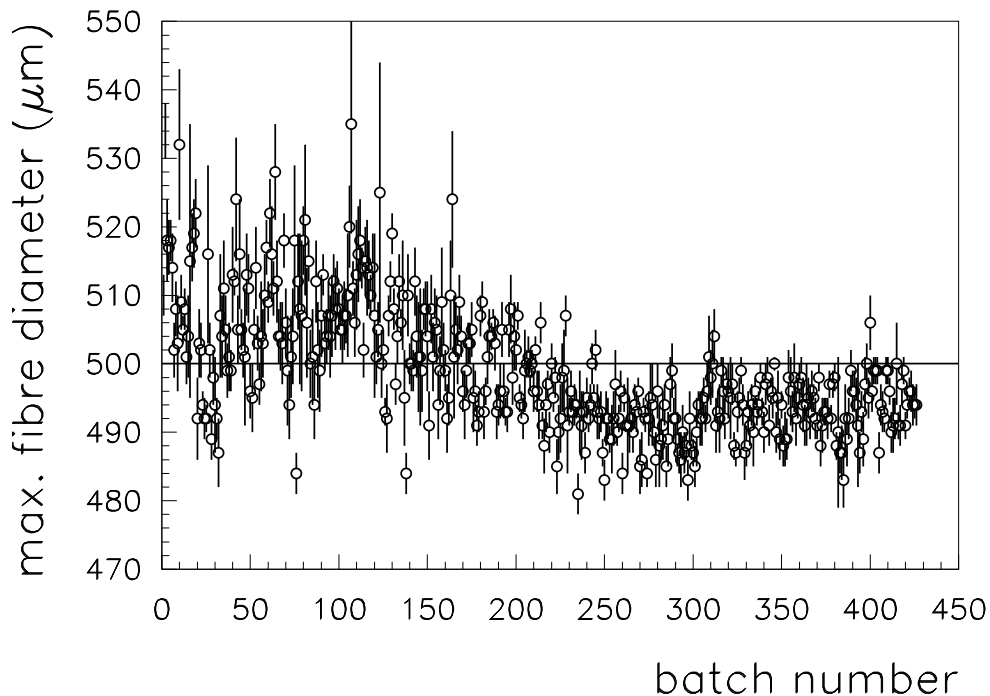
Figure 7: Average fibre diameters as function of the batch production order.

Additional studies showed that the light transmission in the fibres is seriously reduced by mechanical pressure [22]. To avoid any pressure on the fibres, the fibres have to fit well into the lead grooves. The specified variation of the fibre diameters was restricted to $0.5^{+0.00}_{-0.02}$ mm. The fibre diameters were routinely checked during module production. In Figure 7 the average maximum diameter of various fibre batches is shown as a function of the batch number, which corresponds to their production order. Starting with average fibre diameters exceeding the nominal diameter, considerable progress was subsequently made by the producer such that the bulk of the delivered fibres had diameters fitting well into the specified range.

4.3 2–Cell Module Construction

The smallest construction unit is a 2–cell module. It consists of a stack of 52 lead plates each equipped with 90 fibres. The fibre ends form two 70 mm long fibre bundles ending in an aluminium collar. The cross section of each cell is 40.5×40.5 mm^2. A sketch of a 2–cell module is shown in Figure 8.
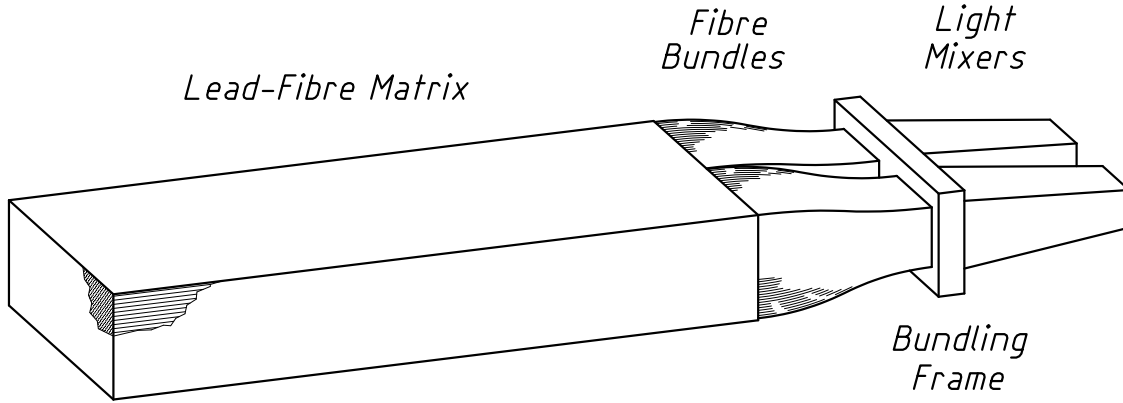

Figure 8: Drawing of a 2–cell module showing lead–fibre matrix, fibre bundles and light mixers. Each fibre bundle contains 2340 fibres.

The first step of the 2–cell module construction is the insertion of the fibres into the grooves of the lead plates. Close to the front of the lead plate the fibres are fixed in the grooves by a thin strip of acrylic glue running perpendicular to the fibres. Without glue the handling of the lead plates during the 2–cell module assembly turned out to be extremely difficult. Since the shower maximum is typically positioned at a depth of 5 cm, possible light attenuation effects due to the influence of this glue on the scintillating fibres is negligible. At the photomultiplier end a 1 cm wide strip of black epoxy glue — again running perpendicular to the fibre direction — absorbs the light in the cladding of the fibres and gives mechanical stability to the stacked plates.

The plates with fibres are then stacked in a form, which is pressed horizontally and vertically with a weight of 1.5 tons. This procedure avoids any subsequent uncontrolled deformation of the assembled detector due to its own weight. It also partially removes remaining air gaps and helps to keep within the specified dimensions of the 2–cell modules. Note that there is no pressure on the fibres, which are protected by the lead structure.

After pressing, the mechanical tolerances of a 2–cell module are typically 0.1 mm in both width and height. An enlarged view of the front of a module in Figure 9 shows the regular pattern of the lead–fibre matrix illuminated by a light source. The different brightness of some fibre ends is an artifact of minimal differences in the fibre orientation, which is irrelevant for the detector performance. For some fibres the thin acrylic cladding can be seen. Note that the fibre diameter is only 0.5 mm.

Next, the fibre ends belonging to the two cells are sorted into two fibre bundles held by an aluminium frame and are glued with a blackened epoxy glue. The fibre bundle end was later machined to ensure homogeneous light readout.
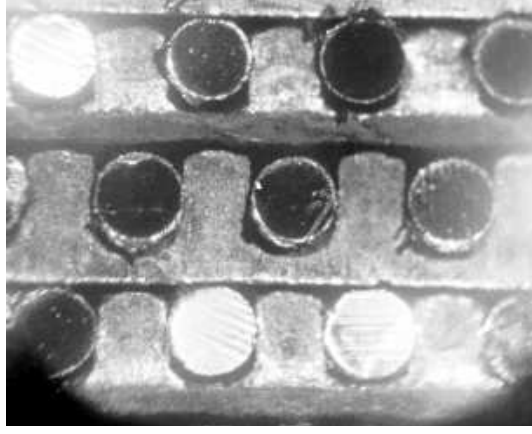
11

Figure 9: Front view of the lead–fibre matrix seen through a microscope.

Finally, the stacked lead plates of the 2–cell modules are stabilized by a layer of 60 μm thick tape surrounding the module.

4.4   16–Cell Module Construction

The main part of the detector consists of sixty 16–cell modules, formed by eight 2–cell modules each. The 16–cell module cross section is 162.6 $\times$ 162.6 mm^2 with a mechanical precision of typically 0.1 mm. This value — similar to that of the 2–cell modules — is obtained by combining 2–cell modules of matching geometrical sizes.

The mechanical stability of a 16–cell module is provided by connecting the bundling frames of adjacent 2–cell modules and by wrapping the module with two layers of 60 μm thick tape. The fibre bundles are protected by a 50 μm thick rectangular steel tube connected to the bundling frames.

The front face of the 16–cell modules is protected by a cushion made of foam material, placed over a 50 μm thick aluminium foil molded on the lead–fibre matrix. The foam is filled with glue which adapts to the shape of the front face before hardening. The cushion is covered by a 50 μm thick steel cap. This protection allows us to put the modules onto their front face and move them easily during assembly without risking deformation of the lead–fibre structure.

The bundle end of the 16–cell module with its 16 fibre bundles is machined to form a flat optical surface. In spite of the different materials of bundling frames and glued fibres, the average surface variation is less than 0.3 μm in height after machining. This ensures well defined optical transmission to the light readout chain that follows.

The 2–cell modules within a 16–cell module are orientated with their lead plates running either horizontally or vertically. Their orientation depends on the 16–cell modules' detector position. It is chosen to minimize 'channeling' — the signal dependence on a particle's impact position caused by the lead–fibre structure which leads to a reduced energy resolution. Channeling effects are an intrinsic property of all lead/scintillating–fibre calorimeters [23]. They are largest if the incident particle direction is parallel to the fibre orientation. Due to the limited geometric acceptance of the calorimeter, this case does not occur for particles originating from the H1 interaction point. Higher–order channeling might, however, be present to some extent for particles traversing the lead–fibre matrix parallel to its symmetry planes. This happens for

electrons impinging on the calorimeter at azimuthal angles of 0°, 60° and 120° with respect to the lead plates. As can be seen from Figure 3, the 2–cell modules are arranged in such a way that those critical angles are avoided.

Beside the 16–cell modules described above, five different types of special modules have been built to approximate the circular shape of the aluminium frame surrounding the detector. Some of these modules have reduced cell sizes and some of them are of non–rectangular shape. The corresponding bundling frames, the number of fibres per bundle and the position of the photomultiplier housings are slightly modified as well.

Similarly, special modules approximating the shape of the beam pipe were built. These modules are of major importance since they cover the interesting kinematical region of very low x and Q^2 values. Their construction is described in detail in the next section.

4.5   Insert Module

The innermost module of the electromagnetic calorimeter which surrounds the beam pipe is called the insert module. The insert module has the same outer size as a 16–cell module and it also consists of 16 cells. The insert cells are not rectangularly shaped in order to allow for the space needed for the beam pipe. An r−ϕ view of the insert module is sketched in Figure 10.
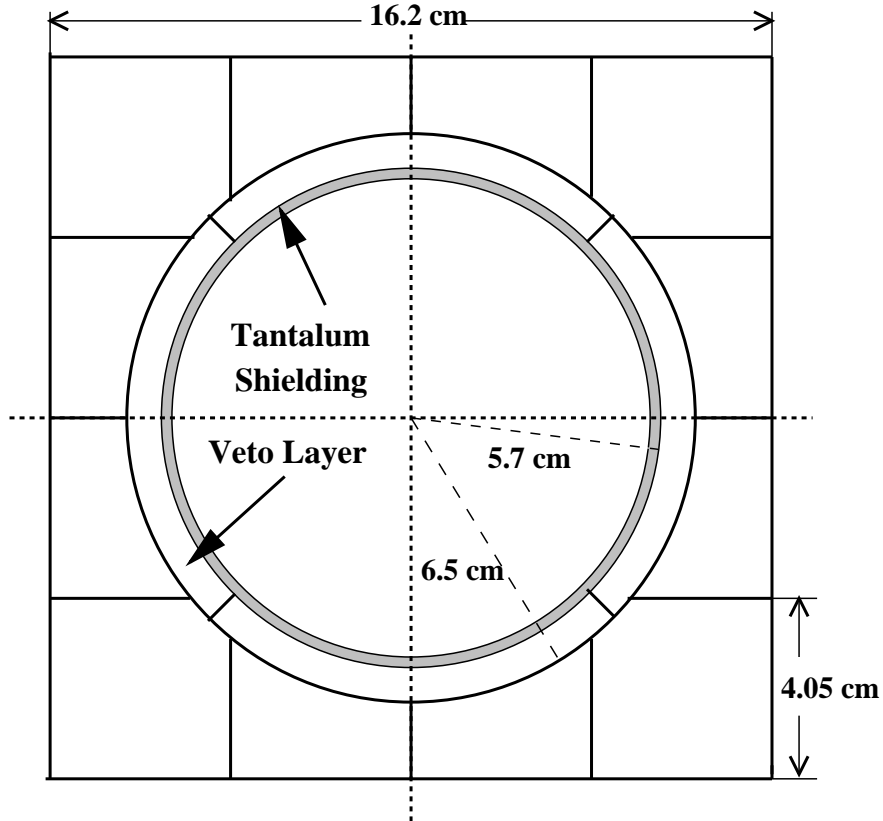

Figure 10: r−ϕ view of the insert module.

The four inner cells surrounding the beam pipe — the veto layer cells — are 8 mm thick. Their purpose is to detect energy leakage of the neighbouring cells into the beam pipe. Furthermore they allow us to identify events where the scattered electron hits the beam pipe inside

13

the calorimeter. The outer radius of the veto layer is 65 mm measured from the center of the beam pipe. This corresponds to a scattering angle of approximately 177.5° at normal running conditions.

Mechanically, the insert is divided into four quadrants. This allows convenient assembly of the insert modules after the main part of the calorimeter is already installed in its final position in the H1 detector. Each quadrant consists of a stack of lead plates. The separation of the quadrants is indicated by the dotted lines in Figure 10. Note that each veto layer cell consists of two lead/scintillator parts belonging to different quadrants. It is, however, read out by one photomultiplier.

The special shape of the insert cells is achieved by cutting normal size lead plates to the required dimensions, filling them with fibres and stacking the equipped plates in a suitable stacking form. The procedure is similar to the production of 2–cell modules. The small size of the insert cells implies that the photomultiplier housing, the shape of the light mixers and the size and form of the fibre bundles are modified compared to the normal 2–cell modules.

A 2 mm thick tantalum layer protects the active detector elements from synchrotron radiation. Tantalum was chosen because it combines high shielding density with good mechanical stability.

4.6   Quality Control of Detector Modules

To control the quality of the detector modules we built a β–source test station [24, 25]. The front of the modules was irradiated by a collimated ^{90}Sr β–source of 40 MBq activity. The source was mounted on a stepper motor of 10 μm precision which was typically moved in 1–2 mm steps in the vertical and horizontal direction, covering an area of 120 × 120 mm^2. For each scan position, the scintillation light produced by the β–electrons was measured by a digital ammeter measuring the photomultiplier current. The set–up and the measurement were controlled by a computer.

Due to the limited range of the β–electrons, which probe the surface of the modules only, scintillation light is produced close to the front end of the fibres. The scan then provided valuable information on the homogeneity of light transport along the fibres. As a typical example, a contour plot of the detector response is shown in Figure 11. The number of contour lines characterizes the deviation below the average detector response. Deviations above the average detector response are not shown. Each contour line corresponds to a deviation of 4%. The plot shows no significant inhomogeneities at the cell boundaries within 2–cell modules. There are inhomogeneities over a zone of a few mm around the vertical border of different 2–cell modules. These inhomogeneities are of the order of 10% for the 16–cell module shown. Note that the homogeneity of modules probed with a β–source can not be directly compared to that seen by an extended electromagnetic shower. In general, a decrease of 10% detector response along 2–cell module boundaries corresponds to an effect of less than 2% for an electron beam of a few GeV energy, which can easily be corrected in off–line analyses.

All 16–cell modules were checked in the test station. The first four modules that were produced showed poorer homogeneity than the following ones and were rejected. The test results of the other 16–cell modules were used to optimize their position in the detector, e.g. the best modules were placed at small radii from the beam, where the deep inelastic scattering cross section is largest. For a module of high quality, the RMS of the detector response averaged over an area of 120 mm × 120 mm is typically 7%. We also measured the light yield averaged over the cell centers for all cells. The average light yield per cell shows a typical cell–to–cell

variation of 6%. The observed spread is consistent with the variation of the average light yield for different fibre batches.
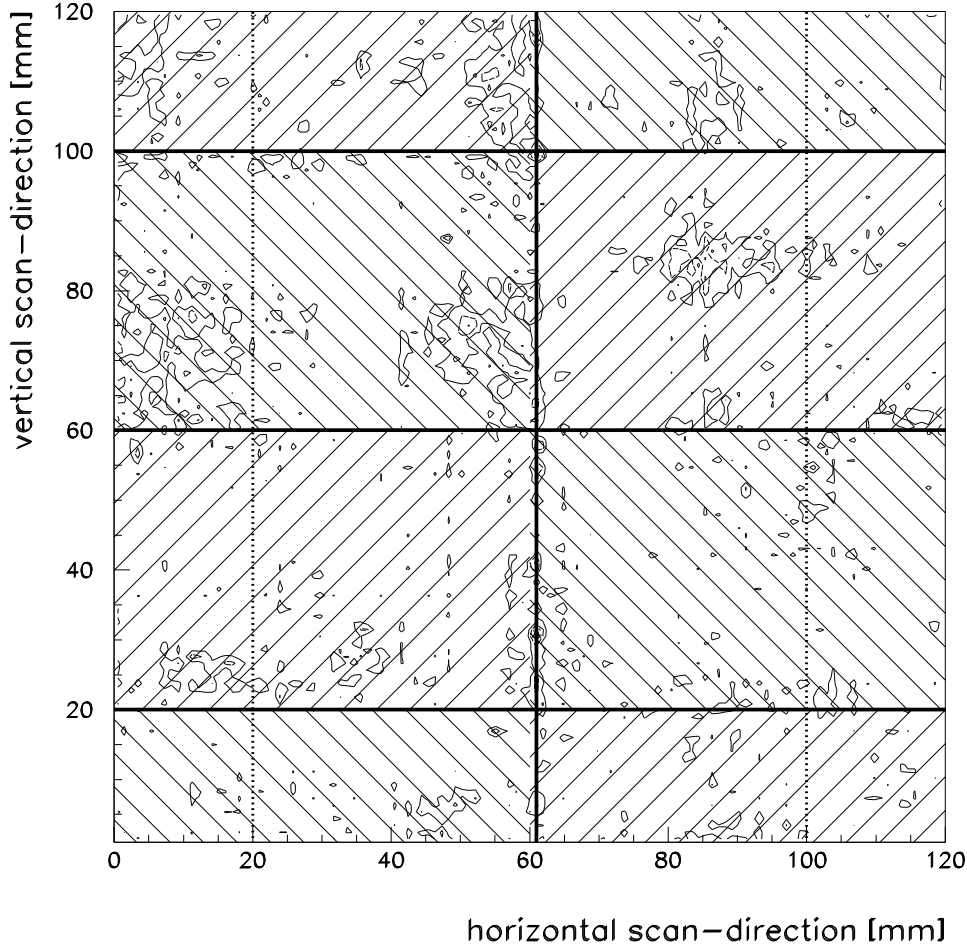

Figure 11: Homogeneity profile of a 16–cell module with β–electrons. Each contour line corresponds to a deviation of 4% from the mean detector response. The hatching indicates different 2–cell modules. Boundaries between 2–cell modules are indicated by the bold lines. The cell boundary inside each 2–cell module is shown as a dotted line.

4.7 Light Readout Chain and Gain Monitoring System

Efficient light transport and readout without any losses or inhomogeneities is of major importance for the energy resolution of the calorimeter. In this section, the photomultiplier, the choice of light mixer and the photomultipler gain monitoring system is described.

The core of the light readout chain is the fine–mesh photomultiplier, Hamamatsu R5505 [26]. This photomultiplier provides a gain of the order of 10^4 in the magnetic field of 1.0 Tesla where the detector is operated. The cathode sensitivity is maximal for a wavelength of 420 nm, which is well matched to the peak of the emission spectrum of BCF–12 scintillating fibres at 430 nm. The transit time spread of 0.35 ns is well below the 1 ns time resolution we aim for. The outer diameter of the photomultipliers is 1 inch for the electromagnetic calorimeter and 2 inches for the hadronic one. This is small enough to allow placing each photomultiplier directly behind its corresponding lead/fibre matrix.

Each of the 1192 photomultipliers of the electromagnetic section and of the 136 photomultipliers of the hadronic section were subjected to detailed quality control checks. Photomultipliers with insufficient gain, poor photocathode homogeneity or other defects were identified and exchanged [27]. Measurements of photocathode homogeneities of the photomultipliers of the electromagnetic calorimeter showed that the variation of the photomultiplier response corresponds to an RMS of the order of 10% in a magnetic field of 1.0 Tesla. The corresponding value for the larger photomultipliers of the hadronic calorimeter is 15%.

The impact of photocathode non–uniformities is considerably reduced by mixing the scintillation light from the fibres in an acrylic light mixer, which in addition concentrates the light onto the photocathode. The optimal light mixer dimensions were studied by simulations and test beam measurements [28]. We chose a tapered light mixer of square cross section, 26.5×26.5 mm^2 at the fibre bundle end and 14.5×14.5 mm^2 at the photomultiplier end. The smaller cross section at the photomultiplier end is due to the reduced effective size of the photocathode in the magnetic field. The length of the light mixer is 68.6 mm. The optical coupling of the fibre bundle to the light mixer is provided through a 0.3 mm thick air gap, while the light mixer and the photomultiplier are connected by optical glue. For the inner 36 detector cells, we conservatively use the Hamamatsu R5506 photomultiplier, which has a UV glass entry window, and radiation hard quartz light mixers [29].

Each group of 16 photomultipliers, together with bases and light mixers, is contained in a light–tight 16–tube aluminium housing which was blackened by anodization. A drawing of the housing showing one tube in detail is presented in Figure 12.
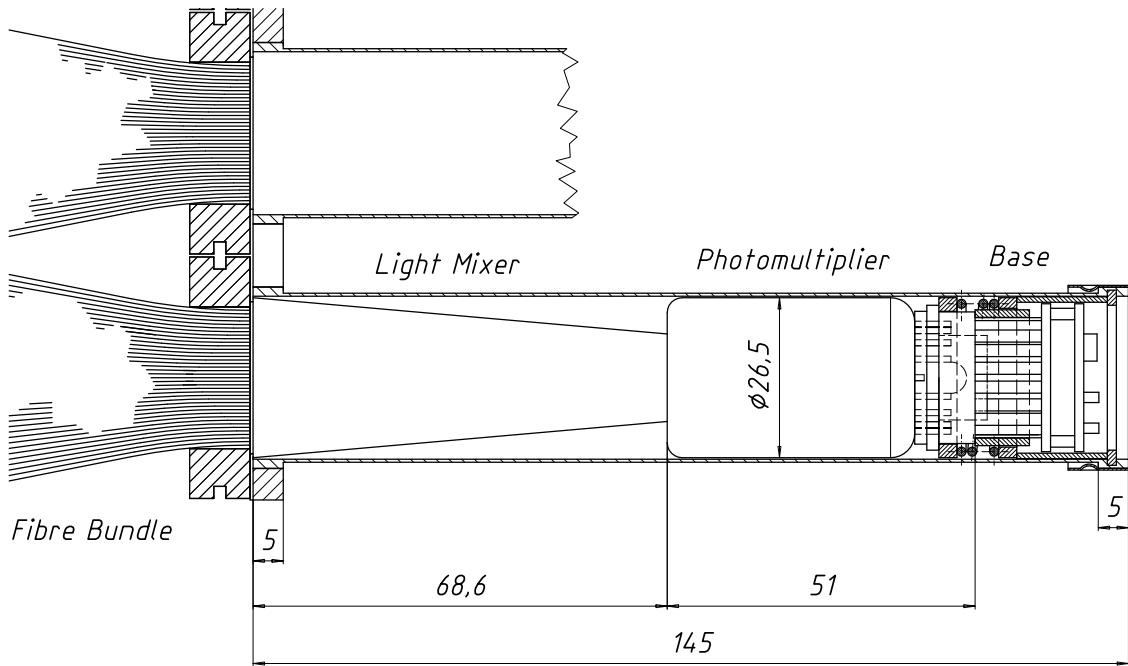
Figure 12: Housing with light mixer, photomultiplier and integrating printed circuit.

In order to achieve a precise energy measurement it is important to monitor any short–term fluctuations and long–term drifts of the photomultiplier gains with a precision of a few per mil. We perform this task by means of a light–emitting diode (LED) monitoring system. This consists of a set of LEDs which are connected via optical fibres to the light mixers and thus

to the photomultipliers. Each LED is linked to eight photomultipliers and to one photodiode. A set of five LEDs and the corresponding photodiodes are contained in a small brass box. In total, 68 boxes are mounted at the back of the electromagnetic calorimeter.

The photodiode measurement is used to identify instabilities of the LED intensity. Thus, any change in photomultiplier gain can be detected and corrected offline.

The system provides redundancy by connecting each photomultiplier to two different LEDs, which can be fired independently. Each box of five LEDs is linked by a serial bus connection to an external VME module. For each box, a common pulse length can be selected from eight different options. In addition, any of the five LEDs in a given module can be selected to give light pulses.

Typically the system is operated at a rate of 1 Hz. The shortest pulse length has a rise time and a decay time of 10 ns. More details on the LED calibration system can be found in [30].

4.8 Photomultiplier Bases and High Voltage Supply

The photomultiplier signal is integrated at the output capacitance of the photomultiplier. A double emitter–follower printed circuit placed near the base of the photomultiplier drives the signal via a coaxial cable to the front–end electronics outside the detector. The printed circuit is powered via the same coaxial cable.

The high voltage for the photomultipliers is distributed by high voltage distribution boards which are mounted at the back of the photomultiplier housings. The design of the high voltage boards follows the description in reference [31]. Each board is connected to an external high voltage line and supplies a group of at most 16 photomultipliers with high voltage. The high voltage of these 16 photomultipliers can then be varied individually within a range of 350 V using opto–couplers. For each group the photomultipliers were selected such that equal gains can be adjusted within the available high voltage range. The desired high voltage values are transmitted by a serial bus system from an external VME module to the high voltage boards. With this system only 75 external high voltage channels are required to operate the calorimeter. Most high voltage values are in the range of 1700 to 1900 V when the magnetic field is on.

4.9 Assembly of the Electromagnetic Section

The assembly of the calorimeters was performed in three steps. First the 16–cell modules and special border modules were arranged in an 8 mm thick aluminium frame. For convenient handling of the modules, the calorimeter was not oriented vertically as in its final detector position but horizontally, and the modules were put on their front faces. A double layer of 50 μm thick Kapton foil was put between the 16–cell modules. The four 2×25 μm thick steel bands carrying the four modules above the beam pipe were then inserted.

Next, the remaining empty areas between the outer modules and the aluminium frame were filled with tailored Rohacell blocks and epoxy glue. Thus the detector blocks and the aluminium frame formed a solid mechanical unit.

The second major task in detector assembly was the mounting of the photomultiplier housings and the cabling work on the detector. To access the back of the detector, the detector was turned into a vertical position. Due to the modular structure of the detector, the preassembled photomultiplier housings could easily be mounted onto the bundling frames. The space between the tubes of the photomultiplier housings contains a water cooling system and houses the signal cables, high voltage cables and the cables of the light calibration system. The cooling system

consists of 6 mm diameter copper tubes which are connected with bronze clips to the housings. The high voltage supply boards and the light calibration modules are fixed at the back of the photomultiplier housings.

In order to install the electromagnetic calorimeter section in the H1 detector, the four detector modules directly above the beam pipe were removed, and the detector was raised to its final vertical position. The removed modules were reinstalled and the assembled calorimeter was moved on rails into its final position, inside the H1 detector. Last, the quadrants of the insert modules were installed.

5   Hadronic Section

The structure of the hadronic calorimeter section is similar to that of the electromagnetic one. The calorimeter consists of 136 detector modules surrounding the beam pipe. The cross section of the 120 inner modules is 119.3×119.0 mm^2. The sixteen edge modules are specially shaped to approximate the circular shape of the aluminum frame which contains the calorimeter. The six modules above the beam pipe are held by four 2×25 μm thick steel bands fixed at the top of the aluminium frame. These modules can be lifted and removed to install the hadronic calorimeter into the H1 detector as is done for the electromagnetic calorimeter. An r$-\phi$ view of the hadronic calorimeter is shown in Figure 13.
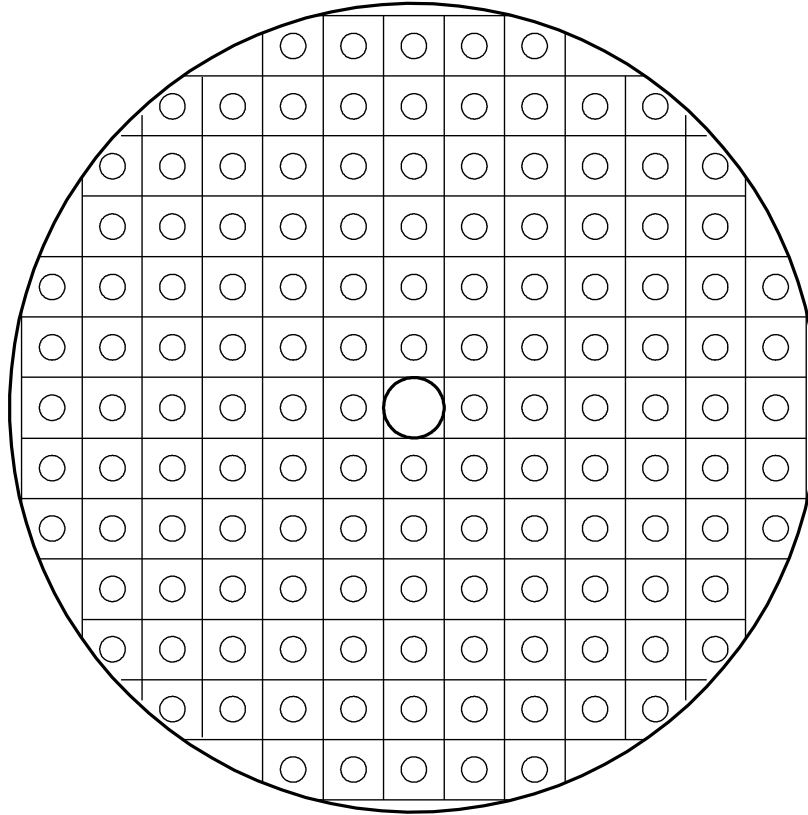

Figure 13: $r - \phi$ view of the hadronic calorimeter. The small circles inside the cells symbolize the photomultipliers to mark active cells.

The angular coverage of the hadronic calorimeter near the beam pipe is extended by an additional backward plug lead/scintillating–fibre calorimeter which is situated in the iron magnetic flux return yoke. The backward plug calorimeter and eight of the specially shaped edge modules of the hadronic calorimeter were implemented during the winter shutdown 1995/96.

5.1 Lead Plates and Scintillating Fibres

The lead plate profile of the hadronic section is shown in Figure 14. Grooves of 1.1 mm diameter to be filled with 54 fibres of 1 mm diameter per plate are made on both sides of the lead plates. The thickness of the lead plates is 1.9 mm. Due to their coarser structure and larger tolerances, the hadronic plates were produced by extrusion. This has the advantage of being a simple and fast technique and it allowed us to produce the grooves on both sides of the plates in one step, providing regular spacing and good longitudinal alignment.
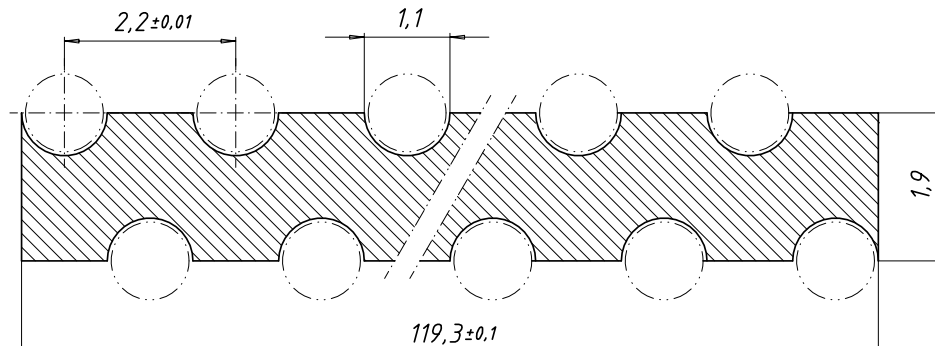

Figure 14: Cross section of a lead plate (hadronic calorimeter).

The active medium in the hadronic calorimeter is 1 mm thick BCF–12 scintillating fibres from BICRON. As in the electromagnetic section, the spectrum of the scintillation light matches the photocathode sensitivity and the fibres have an attenuation length greater than 3 m. Again, the fibres are polished and mirrored at one end to enhance the light yield and to improve the uniformity of the detector response.

5.2 Module Production

The module construction proceeded in the following steps. The fibres were put into the lead grooves and then covered by a thin layer of epoxy glue of 5 mm width running perpendicular to the fibre direction. The stacked modules were pressed with a weight of 1 ton while the epoxy polymerized. The module of stacked plates is wrapped with a foil of 0.1 mm thick stainless steel, which keeps the module light–tight and mechanically rigid. The steel foil is welded by an industrial laser–welding machine. A side view of a hadronic module including the photomultiplier housing is given in Figure 15.

A module contains in total 3510 fibres, which are bundled and held by an aluminium frame. The fibre bundles are 90 mm long. They were glued to the aluminium frame and subsequently machined and polished. A 1.5 mm thick steel frame covering the fibre bundle gives mechanical stability and helps to shield from synchrotron radiation.

Each fibre bundle is coupled via an 80 mm long acrylic light mixer to a 2 inch photomultiplier. The light mixer and the photomultiplier are contained in a common aluminium housing. We use the Hamamatsu R2490–06 fine–mesh photomultiplier [26], which provides a gain of the order of 10^5 in the magnetic field of 1.0 Tesla where the detector is operated. The light mixer has a square cross section with 60 mm sides at the fiber bundle end and transforms to a cylindrical shape of 32 mm diameter at the photomultiplier end. It is coupled by a 1 mm air gap to the fibre bundle and is glued to the photomultipler entry window.
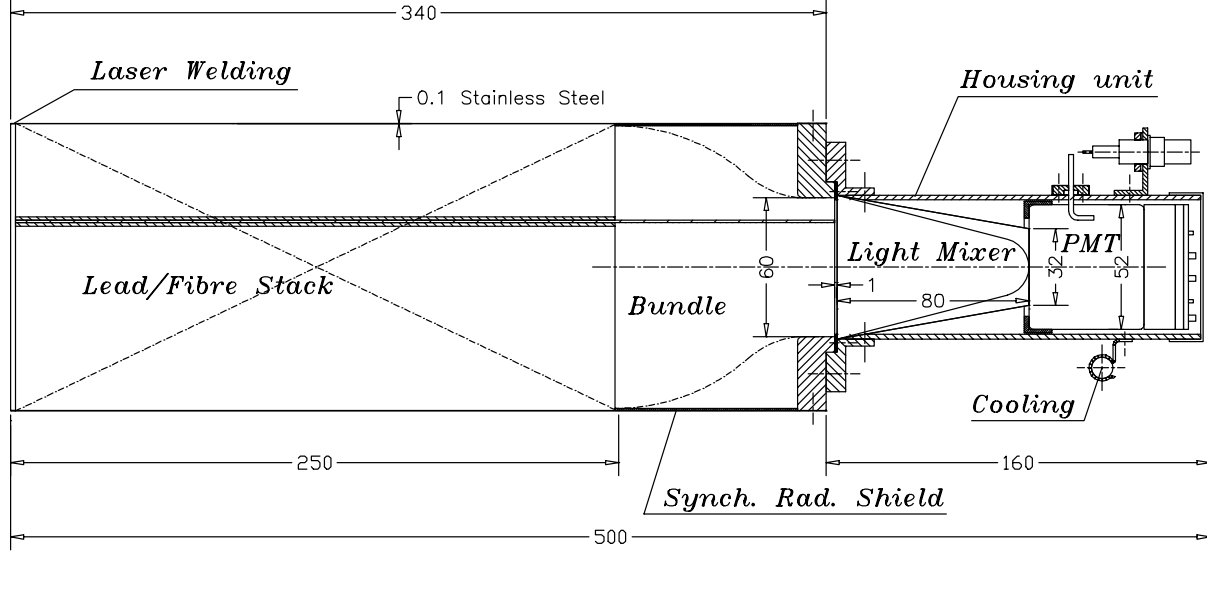

Figure 15: Side view of a hadronic calorimeter module.

The quality of the production modules was measured using cosmic muons triggered by a set of scintillation counters which defined three vertical slices parallel to the longitudinal axis of the modules. The detector response to the muons in these slices is digitized and read out by a computer. The set–up provided information on light yield fluctuations from module to module and determined the size of possible inhomogeneities within a single module, which were found to be typically 3.5%.

5.3   The Backward Plug Calorimeter

The backward plug calorimeter consists of 12 modules with a minimum radial distance of 6 cm to the beam centre. It is positioned at a distance of 2620 mm from the nominal interaction point, and is shown in Figure 16.

The backward plug calorimeter fulfills several tasks. The large distance of the calorimeter from the ep collision vertex ensures a high discrimination power for out–of–time proton beam–related background events. It thus provides additional veto information to the H1 first level trigger. Furthermore, it extends the acceptance of the electromagnetic and hadronic calorimeter to polar angles of 178.7°, covering a Q^2 range of approximately $0.1 - 0.5$ GeV^2 for events at the nominal ep interaction vertex. Therefore, the backward plug extends the coverage of the main electromagnetic and hadronic calorimeter sections into the transition region between deep inelastic scattering and photoproduction processes.
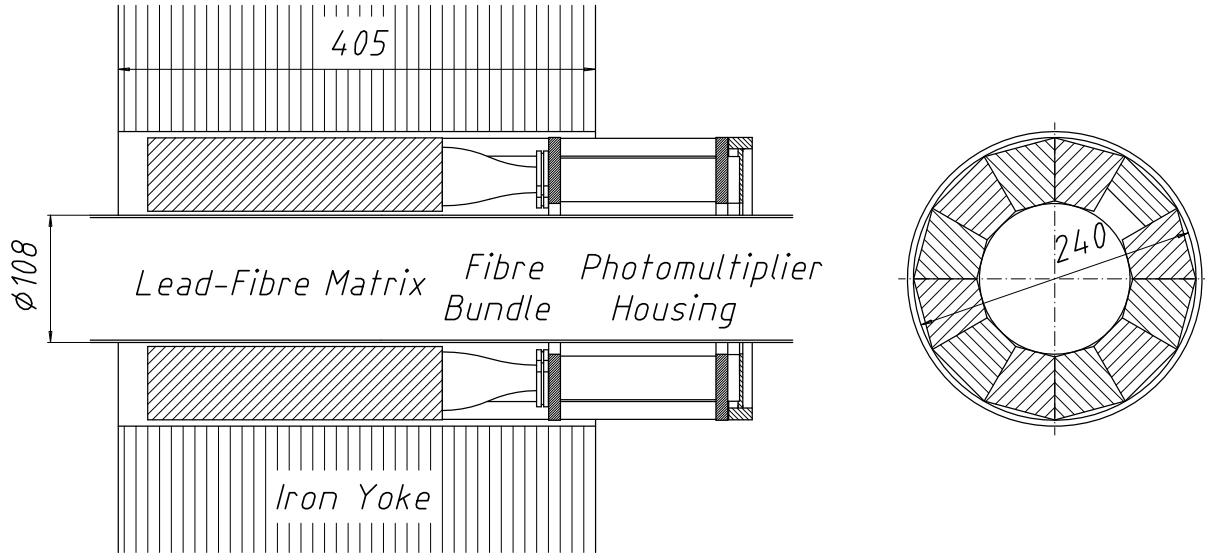
20

Figure 16: Side view and r−ϕ view of the backward plug calorimeter. The height of the modules is 51.6 mm. The module in the upper right part of the r−ϕ view is irregularly shaped to leave space for the feed–throughs of a beam pick–up antenna.

The backward plug calorimeter modules were built up in a similar manner to the hadronic calorimeter modules. Their lead–to–fibre ratio is 3.4:1 and 1 mm thick fibres are used. The modules have a trapezoidal cross section to ensure full coverage in ϕ. The backward plug calorimeter consists of two half–shells that are housed in the correponding shells of the iron return yoke of the H1 magnet. We use the same photomultiplier type as for the electromagnetic section due to space restrictions. The high voltage supply and the calibration system are set up in the same way as for the main part of the hadronic section.

6 Summary

The design parameters and the construction of the H1 lead/scintillating– fibre calorimeter have been presented. The ambitious requirements on energy, timing and position resolution, combined with good electron–pion separation and hadronic energy measurement, led naturally to the novel combination of 0.5 mm fiber diameter with a lead–to–fiber ratio of 2.3:1 for the electromagnetic section and to the construction of a separate hadronic calorimeter.

Solutions to the technical challenges caused by this choice were found and the calorimeter was successfully installed in the H1 detector during the winter shutdown 1994/1995. Test beam measurements as well as the experience of the first year of data taking indicate that the design goals have essentially been reached.

7 Acknowledgements

It is a pleasure to thank all engineers and technicians from the participating institutes for their outstanding commitment and their good team spirit. Their excellent work made the successful

realization of the SPACAL project possible. We would also like to thank Sternwarte Bergedorf for the good cooperation and their valuable help in mirroring the fibres.

References

[1] H1 Collaboration, *Technical Proposal to Upgrade the Backward Scattering Region of the H1 Detector*, PRC 93/02, March 1993.

[2] H1 Collaboration, I. Abt *et al.*, DESY–96–01, March 96, submitted to Nucl. Instr. and Meth.

[3] H1 SPACAL Group, R. D. Appuhn *et al.*, DESY–96–013, Jan. 1996.

[4] H1 SPACAL Group, *The Electronics of the H1 Lead/Scintillating–Fibre Calorimeter*, to be submitted to Nucl. Instr. and Meth.

[5] H1 SPACAL Group, E. Barrelet *et al.*, Contributed Paper for the 1995 EPS Conference.

[6] H1 SPACAL Group, T. Nicholls *et al.*, DESY–95–165, Sept. 1995, to appear in Nucl. Instr. and Meth. **A374** (1996).

[7] H1 SPACAL Group, R. D. Appuhn *et al.*, DESY–95–250, Dec. 1995, submitted to Nucl. Instr. and Meth.

[8] H1 Collaboration, T. Ahmed *et al.*, Nucl. Phys. **B439** (1995) 471.

[9] R. D. Appuhn *et al.*, Nucl. Instr. and Meth. **A350** (1994) 208.

[10] H. Burmeister *et al.*, Nucl. Instr. and Meth. **A225** (1984) 530.

[11] H. Blumenfeld *et al.*, Nucl. Instr. and Meth. **A225** (1984) 518.

[12] P. Sonderegger, Nucl. Instr. and Meth. **A257** (1987) 523.

[13] NA38 Collaboration, A. Devaux, Nucl. Phys. **A498** (1989) 509.

[14] DELPHI Collaboration, P. Aarnio *et al.*, Nucl. Instr. and Meth. **A303** (1991) 233.

[15] D. W. Hertzog *et al.*, Nucl. Instr. and Meth. **A294** (1990) 446.

[16] KLOE Collaboration, A. Aloisio, *The Kloe Detector Technical Proposal*, LNF–93/–002, Jan. 1993.

[17] D. Acosta *et al.*, Nucl. Instr. and Meth. **A294** (1990) 193;
D. Acosta *et al.*, Nucl. Instr. and Meth. **A302** (1991) 36;
D. Acosta *et al.*, Nucl. Instr. and Meth. **A305** (1991) 55;
D. Acosta *et al.*, Nucl. Instr. and Meth. **A308** (1991) 481;
D. Acosta *et al.*, Nucl. Instr. and Meth. **A309** (1991) 143;
D. Acosta *et al.*, Nucl. Instr. and Meth. **A314** (1992) 431;
D. Acosta *et al.*, Nucl. Instr. and Meth. **A316** (1992) 184;
D. Acosta *et al.*, Nucl. Instr. and Meth. **A320** (1992) 128.

[18] RD1 Collaboration, J. Badier *et al.*, Nucl. Instr. and Meth. **A337** (1993) 314;
RD1 Collaboration, J. Badier *et al.*, Nucl. Instr. and Meth. **A337** (1993) 326;
RD1 Collaboration, L. Linssen, Nucl. Instr. and Meth. **A344** (1994) 73.

[19] BICRON, 12345 Kinsman Road, Newbury, OH 44065, USA.

[20] R. Barschke, Diploma Thesis, University of Hamburg, Germany, unpublished, 1994.

[21] J. Cvach *et al.*, Internal Note H1–06/95–443, July 1995.

[22] A. Schuhmacher, Diploma Thesis, University of Dortmund, Germany, unpublished, 1994;
T. Wenk, Diploma Thesis, University of Dortmund, Germany, unpublished, 1994.

[23] M. Livan, V. Vercesi and R. Wigmans, *Scintillating–Fibre Calorimetry*, CERN 95–02, Feb. 1995.

[24] D. Lacour, Diploma Thesis, LPNHE, University of Paris VI–VII, unpublished, 1992.

[25] F. Lehner, Diploma Thesis, University of Hamburg, Germany, unpublished, 1994.

[26] HAMAMATSU PHOTONICS K.K., 314–5, Shimokanzo, Toyooka–village, Iwata–gun, Shizuoka–ken, 438–01 Japan.

[27] A. Heck, Diploma Thesis, University of Heidelberg, Germany, unpublished, 1995;
H1 SPACAL Group, *Series Tests of Fine–Mesh Phototubes in Magnetic Fields of up to 1.2 Tesla*, to be submitted to Nucl. Instr. and Meth.

[28] T. Deckers, Diploma Thesis, University of Dortmund, Germany, unpublished, 1994;
A. Hatzenbühler, Diploma Thesis, University of Heidelberg, Germany, unpublished, 1995.

[29] Radiation hard Glass, Type K5 G20 from Schott Glaswerke, Hattenbergstraße 10, D-55122 Mainz, Germany.

[30] H1 SPACAL Group, *The LED based Calibration System of the H1 Lead/Scintillating–Fibre Calorimeter*, to be submitted to Nucl. Instr. and Meth.

[31] W. Stamm *et al.*, Nucl. Instr. and Meth. **A328** (1993) 601.